Supporting Information

A binary solvent study with n-butanol and dimethyl sulfoxide on PEAI passivation of wide-bandgap perovskite solar cells

Wenda Li[a], Yansheng Sun[a], Kexiang Wang[b], Tingting You[a,*], Yukun Gao[a], Penggang Yin[a,*]

[a] *Key Laboratory of Bio-inspired Smart Interfacial Science and Technology of Ministry of Education, School of Chemistry, Beihang University, Beijing 100191, China*

[b] *School of Energy and Power Engineering, Beihang University, Beijing 100191, China*

**Corresponding author*

E-mail address: youtt@buaa.edu.cn, pgyin@buaa.edu.cn

1. Experiment

1.1 Materials

NiO_x nanoparticles (99.999%), methylammonium bromide (MABr, 99.9%), [4-(3,6-Dimethyl-9H-carbazol-9-yl)butyl]phosphonic Acid (Me-4PACz, 99%) and lead iodide (PbI_2, 99.9%) were purchased from Advanced Election Technology Co., Ltd., and were used without further purification. Lead bromide ($PbBr_2$) were purchased from J&K Scientific Corp in China. Cesium iodide (CsI, 99.5%), 2-Phenylethylamine Hydroiodide (PEAI), C60 and bathocuproine (BCP, 99.9%) were purchased from Xi'an Polymer Light Technology Corp in China and used as received. Formamidinium iodide (FAI, 99.5%) was purchased from Greatcell Solar Materials. Dimethylformamide (DMF), dimethyl sulfoxide (DMSO), chlorobenzene (CB), isopropanol (IPA) and n-butanol (nBA) were procured from Sigma-Aldrich.

1.2 Characterizations

The morphological and structural properties of the films were investigated using a suite of characterization techniques. Scanning electron microscopy (SEM) was performed on a ZEISS Gemini SEM 360 instrument at an accelerating voltage of 5 kV to examine the surface topography. The crystalline structure was analyzed by X-ray diffraction (XRD) on a Shimadzu XRD-6000 diffractometer equipped with a Cu K_α radiation source. Surface roughness was evaluated via atomic force microscopy (AFM) using a Dimension Icon instrument (Bruker). The chemical composition and valence states of the film surface were probed by X-ray photoelectron spectroscopy (XPS) with a Thermo Scientific ESCALAB 250Xi system. Optical properties were assessed through several spectroscopic methods. Ultraviolet-visible (UV-vis) absorption spectra were recorded using a Shimadzu UV-3600 spectrophotometer. Steady-state and time-resolved photoluminescence (PL and TRPL) measurements were conducted on an FLS980 spectrofluorometer (Edinburgh Instruments Ltd.), where the perovskite films were excited at a wavelength of 440 nm by a xenon lamp. Furthermore, PL mappings were acquired with a laser confocal PL imaging microscope (Fast FLIM Q2, ISS, Italy) operating at 405 nm and a repetition frequency of 1 MHz under ambient air. The work function and electronic structure were determined by ultraviolet photoelectron

spectroscopy (UPS) on a Thermo Scientific ESCA Lab 250Xi, calibrated against an Au standard. The photovoltaic performance of the fabricated perovskite solar cells (PSCs) was evaluated under standard test conditions. Current density-voltage (J-V) curves were measured with a Keithley 2400 source meter under a calibrated AM 1.5G solar simulator. The active area of the devices was defined by a metal shadow mask (0.0625 cm^2). The external quantum efficiency (EQE) spectra were characterized using a Newport PVE300 system at room temperature in an ambient atmosphere. To quantify the defect density within the perovskite films, the space-charge limited current (SCLC) method was employed by analyzing the dark current-voltage (I-V) characteristics. Finally, the charge transport and recombination dynamics were investigated by electrochemical impedance spectroscopy (EIS) using an electrochemical workstation, with the frequency swept from 1 MHz to 0.1 Hz. All measurements were carried out at room temperature in an ambient environment.

1.3 Device Fabrication

For the composition $(FA_{0.98}MA_{0.02})_{0.95}Cs_{0.05}Pb(1_{0.95}Br_{0.05})_3$, 1.3 M perovskite precursor solution was prepared by mixing FAI, CsI, MABr, Pbl_2 and $PbBr_2$ in DMF: DMSO (4:1 v: v) mixed solvent subject to the stoichiometric ratio.

The glass/ITO substrates (15 Ω sq^{-1}) was cleaned with detergent, deionized water, acetone, and isopropyl alcohol for 15 minutes, respectively, and then exposed to oxygen plasma for 15 minutes. The ITO substrates were spin-coated with the 35 μL as-prepared NiOx solution (1.0 mg/mL in water) for 30 seconds at 1500 rpm, and then annealed for 10 minutes at 150℃. The Me-4PACz solution (1.0 mg/mL in ethanol) was spin-coated onto the glass/ITO/NiOx substrate at 4000 rpm for 30 seconds following 3 hours of stirring. The substrate was annealed for 10 minutes at 100℃ on a hot plate. The perovskite layer was spin-coated onto the as-prepared substrate at 1000 rpm for 8 s, subsequently at 6000 rpm for 30 s, with 180 μL of chlorobenzene (CB) dripped onto the film at the 18 s. The perovskite film is subjected to a 15-minute annealing step at 100℃ on a preheated hotplate. The passivation solution was prepared by adding 5 μL DMSO to 1 mL PEAI solution (1 mg/mL in n-butanol), which was spin-coated on perovskite film at 3000 rpm for 30 s. Finally, C_{60} (24 nm),

BCP (6 nm), and Ag (100 nm) were thermally evaporated in sequence under high vacuum ($2x10^{-4}$ Torr) through a metal shadow mask, defining a device area of 0.0625 cm^2.

2. Hansen solubility parameters (HSP) equation[17-19]

$$R_a = \sqrt{4(\delta_{d1} - \delta_{d2})^2 + (\delta_{p1} - \delta_{p2})^2 + (\delta_{h1} - \delta_{h2})^2}$$

where, δ_d, δ_p, δ_h are the dispersion forces, polar interactions, and hydrogen bonding. For mixed solvents, the effective HSP values can be approximated using a volume-fraction-weighted linear mixing rule, which is commonly applied for qualitative comparison:

$$\delta_{mix} = f_{DMSO}\delta_{DMSO} + (1 - f_{DMSO})\delta_{nBA}$$

Where f_{DMSO} represents the volume fraction of DMSO in the binary solvent mixture, δ_{DMSO} and δ_{nBA} denote the HSP values of pure DMSO and n-butanol (nBA), respectively.

Hansen solubility parameters (HSP) provide a semi-quantitative framework for evaluating solvent-solute interactions by resolving intermolecular forces into dispersive (δ_d), polar (δ_p), and hydrogen-bonding (δ_h) contributions[20]. The interaction distance R_a in Hansen space reflects the affinity between PEAI/Pb-I species and the solvent, where smaller R_a signifies stronger coordination or dissolution ability[21]. The binary solvent therefore tunes the solvent-solute interaction and evaporation kinetics, leading to more effective and uniform surface passivation.

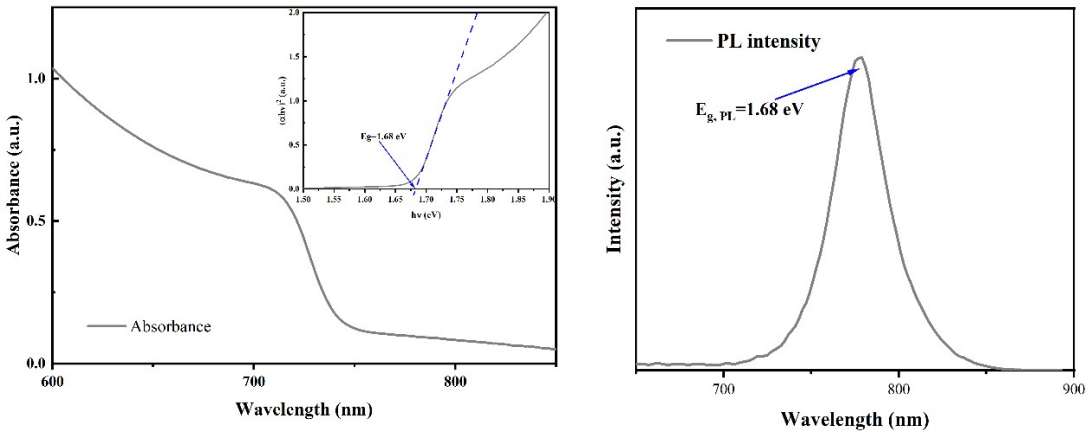

Figure S1. a) UV–vis absorption and b) PL spectra of the perovskite layer.

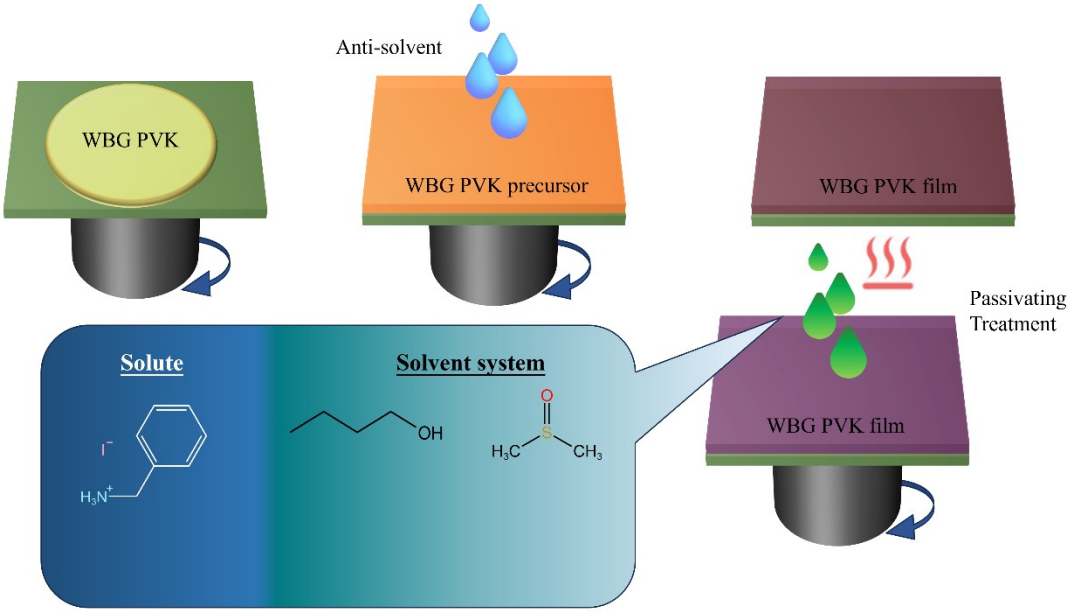

Figure S2. Schematic procedure for the preparation of perovskite films via surface post-treatment under binary solvent strategy with n-butanol and dimethyl sulfoxide.

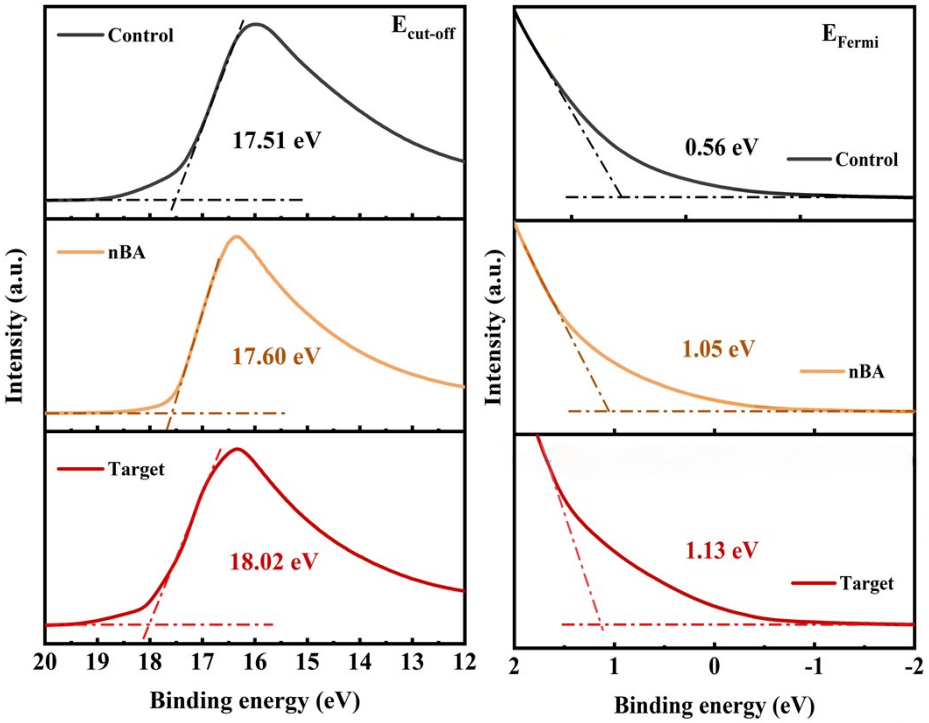

Figure S3. Secondary electron cut-off of the ultraviolet photoelectron spectroscopy (UPS) spectra for the Control, nBA-treated, and nBA/DMSO-treated perovskite films.

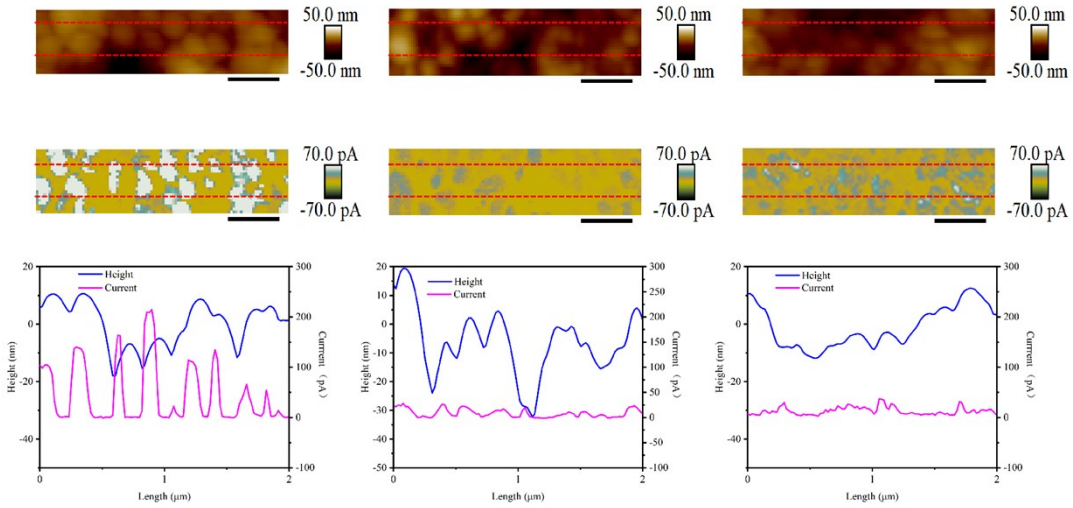

Figure S4. The topographic, current images and the corresponding line profiles measured by c-AFM of Control, nBA and Target perovskite films. The scale bar is 410 nm.

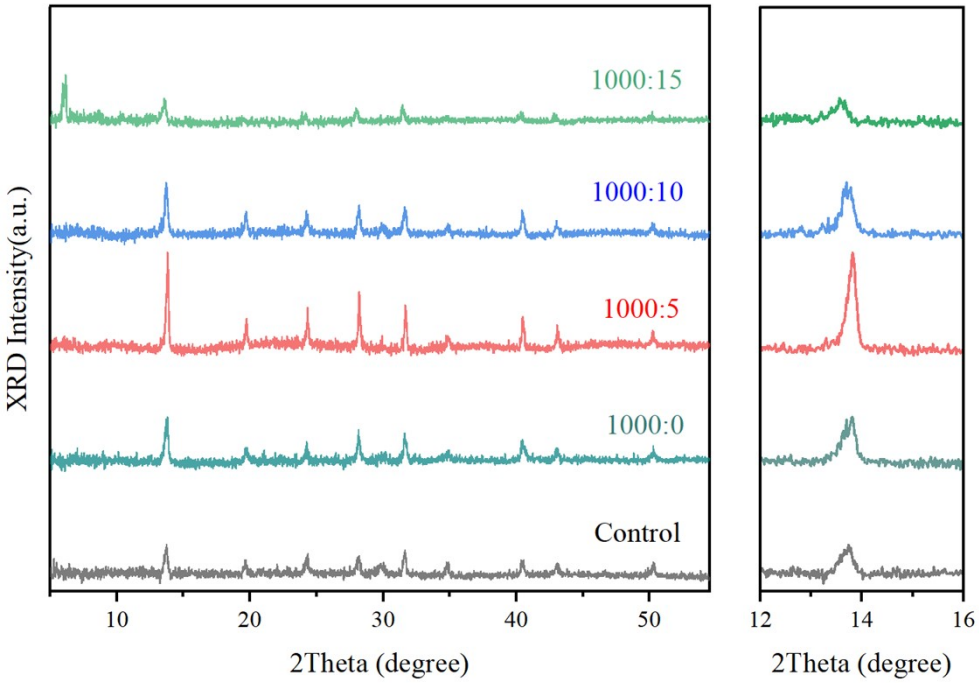

Figure S5. XRD of perovskite films after passivation treatment with different solvent proportions of n-butanol and dimethylsulfoxide.

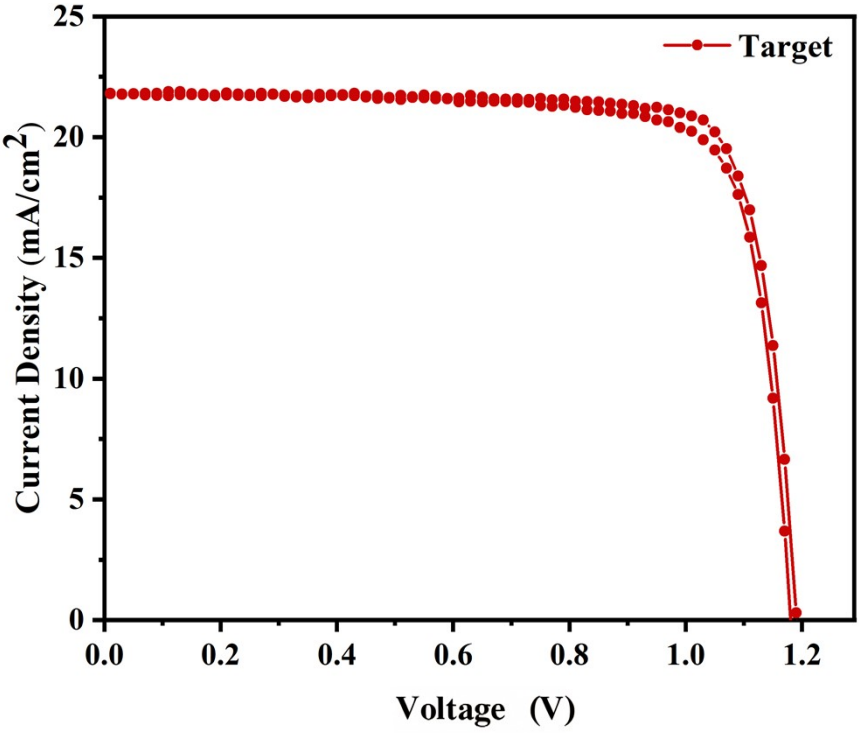

Figure S6. Forward and reverse scan J-V curves of the target devices.

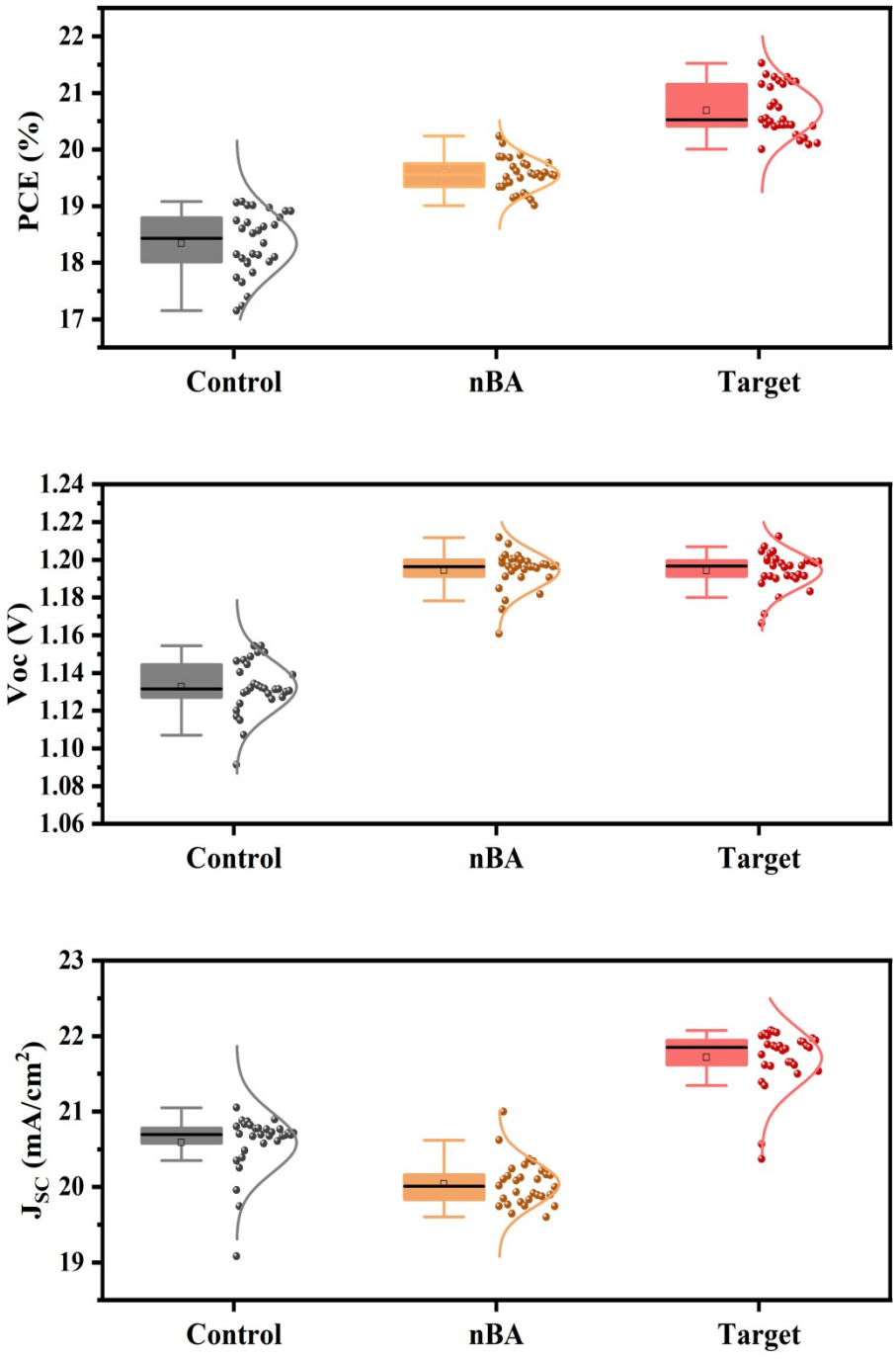

Figure S7. Control, nBA and Target devices with J_{SC}, V_{OC} and PCE parameter boxplots.

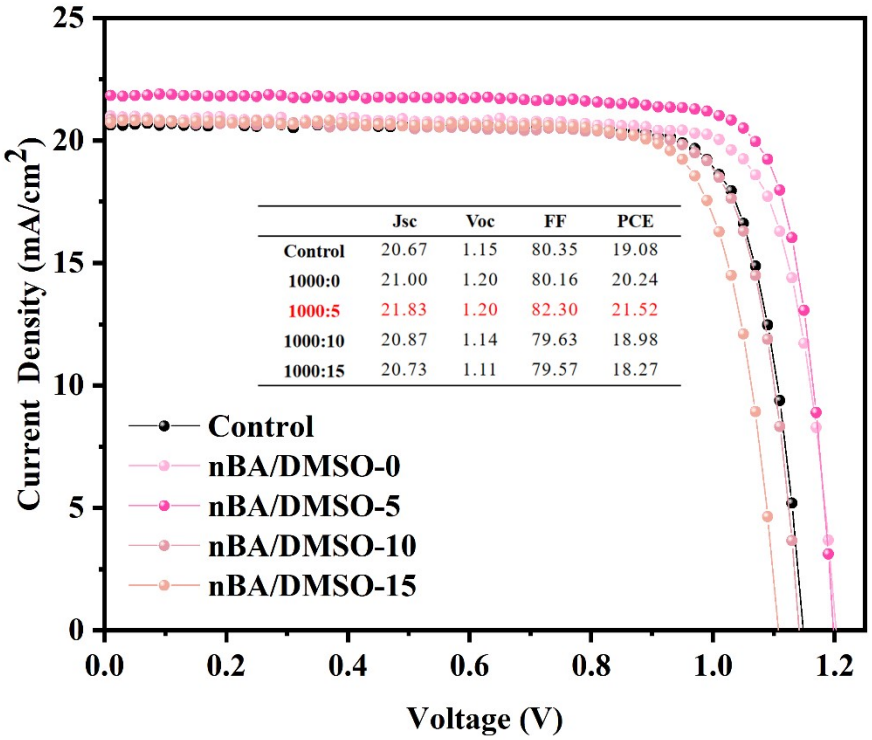

	Jsc	Voc	FF	PCE
Control	20.67	1.15	80.35	19.08
1000:0	21.00	1.20	80.16	20.24
1000:5	21.83	1.20	82.30	21.52
1000:10	20.87	1.14	79.63	18.98
1000:15	20.73	1.11	79.57	18.27

Figure S8. Performance parameters of devices after passivation treatment with different solvent proportions of n-butanol and dimethylsulfoxide.

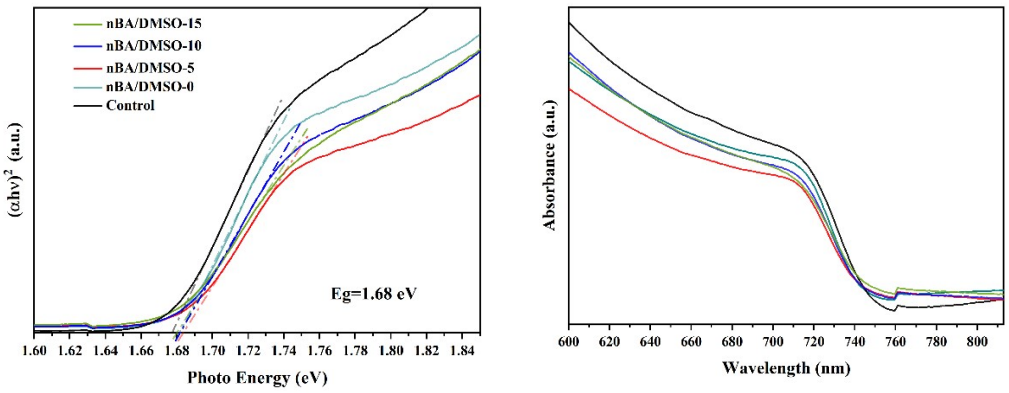

Figure S9. UV-Vis absorption spectra of $Cs_{0.05}FA_{0.8}MA_{0.15}Pb(I_{0.75}Br_{0.25})_3$ films passivated by different solvent ratios.

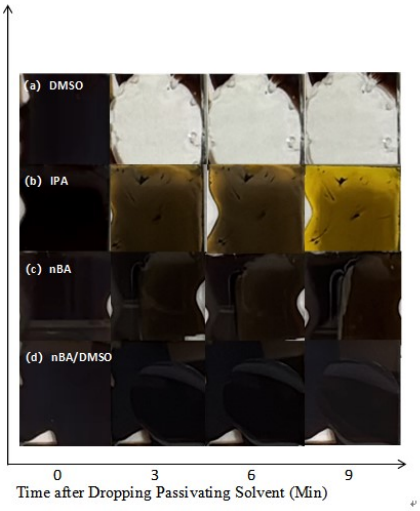

Figure S10. Photographs of the perovskite films after dropping (a) DMSO, (b) IPA, (c) nBA, and (d) nBA/DMSO (1000 μL+5 μL) as passivating solvents.

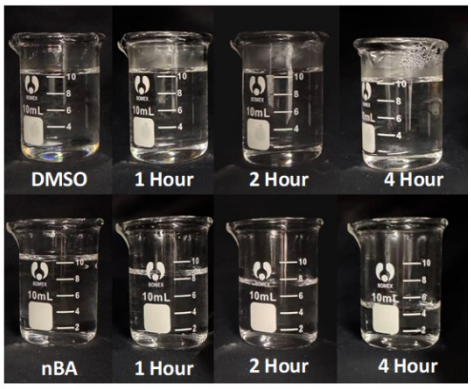

Figure S11. The evaporation rates of DMSO and nBA at a constant temperature of 100℃

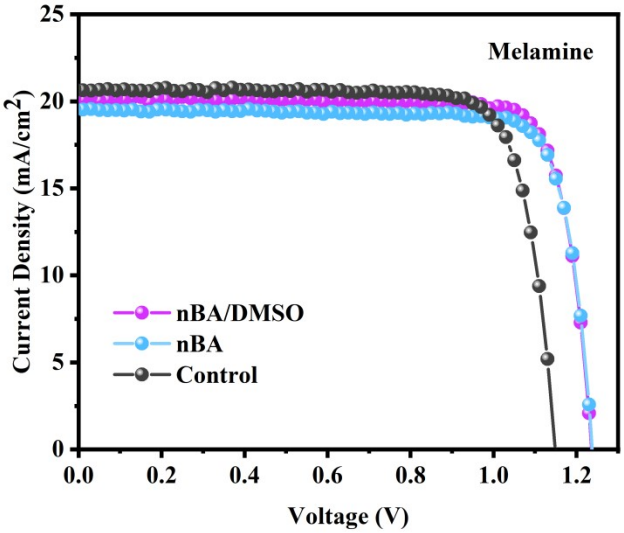

Figure S12. Device performance after Melamine passivation.

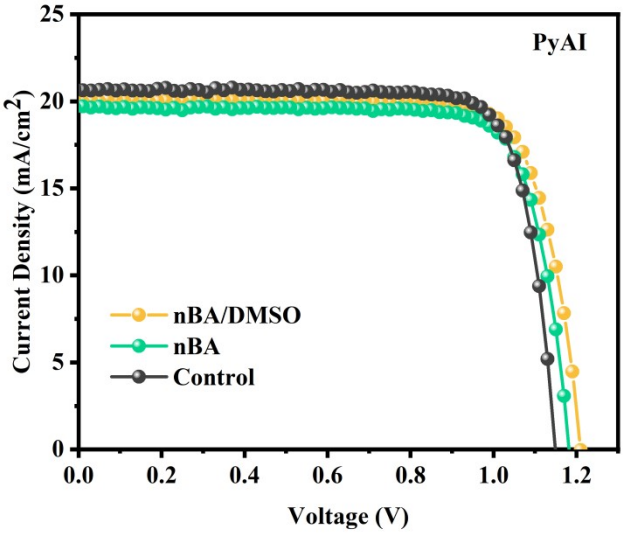

Figure S13. Device performance after 2-Phenylethylamine Hydroiodide (PyAI) passivation.

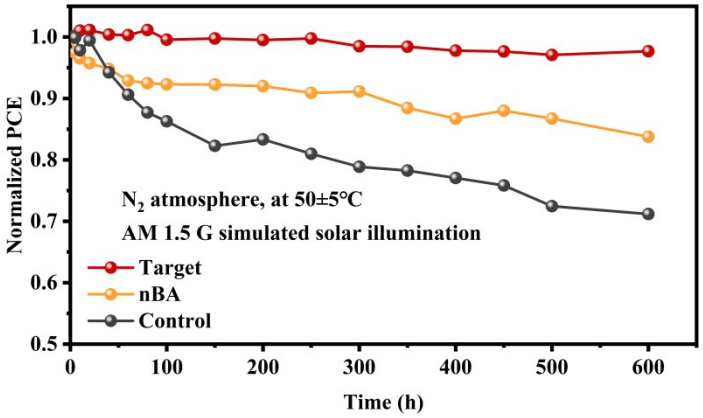

Figure S14. Light-soaking stability of Control, nBA and target PSCs.

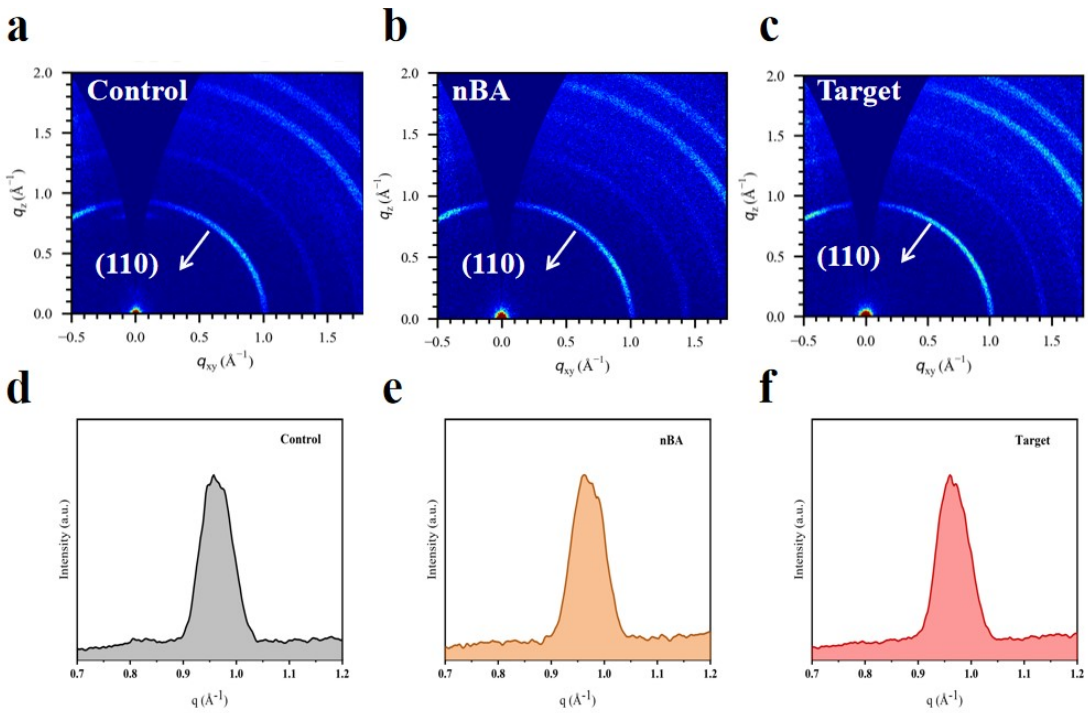

Figure S15. GIWAXS patterns of a) the Control, b) nBA and c) Target perovskite films. The GIWAXS azimuth integral curve graph of d) the Control, e) nBA and g) Target perovskite films.

Table S1. Energy level parameters of perovskite films

	$E_{cut-off}$	W_F	E_{F-edge}	E_{VB}	E_{CB}
Control	17.51	3.71	0.56	-4.27	-2.59
nBA	17.60	3.62	1.05	-4.67	-2.99
Target	18.02	3.20	1.13	-4.33	-2.65

Table S2 Atomic concentration of C_{C-N}, $C_{N-C=N}$, C_{C-C}, N_{C-N} and $N_{N-C=N}$ on the surface of perovskite films.

Sample	Atomic concentration (%)	
	$C_{C-N}/C_{N-C=N}/C_{C-C}$	$N_{C-N}/N_{N-C=N}$
Control	8.78/13.50/77.2	6.75/93.25
nBA	11.18/9.92/78.89	30.31/69.69
Target	12.49/9.57/77.94	36.8/63.2

Table S3 Performance parameters of devices after passivation treatment

	J_{SC} (mA/cm^2)	V_{OC} (V)	FF (%)	PCE (%)
Control	20.67	1.15	80.35	19.08
nBA	21.00	1.20	80.16	20.24
Target	21.83	1.20	82.30	21.52

Table S4. Summary of photovoltaic parameters for WBG PSCs with perovskite bandgap of 1.68 eV in recent years.

Eg (eV)	Voc (V)	PCE (%)	Year	Ref
1.68	1.20	21.52		This work

1.68	1.19	20.3	2023	[1]
1.68	1.187	20.17	2023	[2]
1.68	1.20	20.38	2023	[3]
1.68	1.19	20.31	2021	[4]
1.68	1.202	21.13	2023	[5]
1.68	1.18	20.09	2023	[6]
1.68	1.212	22.17	2024	[7]
1.68	1.199	21.55	2025	[8]
1.68	1.194	18.26	2025	[9]
1.68	1.22	22.46	2025	[10]
1.68	1.19	21.6	2025	[11]
1.68	1.25	22.87	2025	[12]
1.68	1.17	19.80	2019	[13]
1.68	1.18	20.30	2021	[14]
1.68	1.19	21.44	2023	[15]

Table S5. Hansen solubility parameters of representative solvents.

	δ_d	δ_p	δ_h	Notes
N, N-Dimethyl Formamide (DMF)	17.40	13.70	11.30	Standard literature and HSP handbook values[16].
DMSO (dimethyl sulfoxide)	18.40	16.40	10.20	
n-Butanol (nBA)	16.00	5.70	15.80	
Iso-Propyl Acetate (IPA)	14.9	4.5	8.2	

Table S6. Device performance after passivation with various molecules under different nBA-based solvent systems.

Passivation Molecule		J_{SC} (mA/cm^2)	V_{OC} (V)	FF (%)	PCE (%)
	Control	20.67	1.15	80.35	19.08

PyAI	nBA	19.53	1.24	82.26	19.88
	nBA/DMSO	20.15	1.24	82.50	20.55
Melamine	nBA	19.68	1.18	79.17	18.41
	nBA/DMSO	20.01	1.21	79.39	19.22

References

[1] X. Luo, H. Luo, H. Li, R. Xia, X. Zheng, Z. Huang, Z. Liu, H. Gao, X. Zhang and S. Li, *Advanced Materials* **2023**, *35*, 2207883.

[2] J. Cao, Z. Fang and S. Liu, *Solar RRL* **2023**, *7*, 2200955.

[3] H. Guo, Y. Fang, Y. Lei, J. Wu, M. Li, X. Li, H. B. Cheng, Y. Lin and P. J. Dyson, *Small* **2023**, *19*, 2302021.

[4] C. Chen, J. Liang, J. Zhang, X. Liu, X. Yin, H. Cui, H. Wang, C. Wang, Z. Li and J. Gong, *Nano Energy* **2021**, *90*, 106608.

[5] T. Nie, J. Yang, Z. Fang, Z. Xu, X. Ren, X. Guo, T. Chen and S. F. Liu, *Chemical Engineering Journal* **2023**, *468*, 143341.

[6] C. Su, R. Wang, J. Tao, J. Shen, D. Wang, L. Wang, G. Fu, S. Yang, M. Yuan and T. He, *Journal of Materials Chemistry A* **2023**, *11*, 6565-6573.

[7] L. Yang, Z. Fang, Y. Jin, H. Feng, B. Deng, L. Zheng, P. Xu, J. Chen, X. Chen, Y. Zhou, C. Shi, W. Gao, J. Yang, X. Xu, C. Tian, L. Xie and Z. Wei, *Advanced Materials* **2024**, *36*.

[8] X. Zhou, X. Li, B. Shi, P. Wang, X. Du, Y. Zhao and X. Zhang, *ACS nano* **2025**, *19*, 11187-11196.

[9] L. Guo, J. Sun, J. Wang, M. Duan, T. Li, Z. Hu, H. Zhang and Y. Chen, *Advanced Functional Materials* **2025**, *35*, 2422674.

[10] Z. Zhang, Z. Yu, J. Zhao, M. Zhi, W. Dang, Y. Guo, X. Liang, Y. Mai and Z. Li, *Small* **2025**, e2504393.

[11] X. Wang, Z. Lu, L. Zhang, X. Yang, Y. Liu, X. Ji, D. Chi, S. Huang, J. Huang and L. Yang, *ACS Applied Nano Materials* **2025**, *8*, 7787-7795.

[12] Y. Jiang, P. Guo, R. Chen, L. Du, X. Shao, X. Zhang, Y. Zheng, N. Jia, Z. Fang

and L. Ma, *Advanced Energy Materials* **2025**, 2501312.

[13] D. H. Kim, C. P. Muzzillo, J. Tong, A. F. Palmstrom, B. W. Larson, C. Choi, S. P. Harvey, S. Glynn, J. B. Whitaker and F. Zhang, *Joule* **2019**, *3*, 1734-1745.

[14] F. H. Isikgor, F. Furlan, J. Liu, E. Ugur, M. K. Eswaran, A. S. Subbiah, E. Yengel, M. De Bastiani, G. T. Harrison and S. Zhumagali, *Joule* **2021**, *5*, 1566-1586.

[15] X. Niu, N. Li, Z. Cui, L. Li, F. Pei, Y. Lan, Q. Song, Y. Du, J. Dou and Z. Bao, *Advanced Materials* **2023**, *35*, 2305822.

[16] C. M. Hansen, S. Abbott and H. Yamamoto, Hansen Solubility Parameters in Practice (HSPiP), HSPiP Team, **2008-2025**, available at: www.hansen-solubility.com

[17] Hwang M, Cho I W, Lee H, et al. Solvent–Precursor Interaction Engineering for Formamidinium-Based Perovskites: Role of dimethylacetamide, N-Methyl-2-Pyrrolidone, and methylammonium chloride in Film Formation and Device Performance, *Current Applied Physics* **2026**, 83, 15-21.

[18] Bautista-Quijano J R, Telschow O, Paulus F, et al. Solvent–antisolvent interactions in metal halide perovskites, *Chemical Communications* **2023**, 59, 10588-10603.

[19] Chao L, Niu T, Gao W, et al. Solvent engineering of the precursor solution toward large-area production of perovskite solar cells, *Advanced Materials* **2021**, 33, 2005410.

[20] C. M. Hansen, Hansen Solubility Parameters: A User's Handbook, 2nd edn, CRC Press, 2007.

[21] D. F. Fennell, M. J. Wolf, A. J. P. White, et al., Hansen theory applied to the identification of nonhazardous solvents for hybrid perovskite thin-film processing, *Energy Environ. Sci* 2018, 11, 126–135.